Nanotechnology

DOI: 10.1002/anie.201206571

Muscle-like Supramolecular Polymers: Integrated Motion from Thousands of Molecular Machines**

Guangyan Du, Emilie Moulin, Nicolas Jouault, Eric Buhler, and Nicolas Giuseppone**

Dedicated to Professor Sauveur Jean Candau

Endeavors in molecular nanosciences are increasingly directed toward structural and dynamic control of hierarchical self-assembly.[1,2] These lines of research are often inspired by the complexity of living systems that associate molecular and supramolecular organization features in order to self-sustain and to evolve.[3] One of the most intriguing functional properties of living systems is their capacity to produce collective molecular motions and to amplify them by orders of magnitude. For instance, in muscular tissues, the coordinate movements of thousands of myosin heads lead to the gliding of thick myosin filaments along thin actin filaments, and results in a cooperative contraction of the entire sarcomere. In this particular case, the individual shifts of the proteins take place in the 10 nm range, whereas their integrated translation produces a 1 μm contraction of the sarcomeres. Coupling of these micrometric contractions leads to macroscopic motions.[4]

The chemical synthesis of artificial molecular machines (AMMs) is thus of central interest in order to mimic their biological counterparts with the aim of engineering dynamic microscopic devices and macroscopic functional materials by bottom-up approaches.[5–7] To date, a number of seminal reports have outlined the design of individual AMMs that can produce internal motions such as 1) translation in bistable single rotaxanes[8,9] or on molecular tracks,[10] 2) scissor-like motions,[11] and 3) unidirectional circumrotation[12] (in multistation catenanes) or rotation[13,14] (around a central bond) in molecular motors that are driven far from equilibrium by light. In particular, for the design of synthetic molecular muscles, Sauvage and co-workers described the first unimolecular linear array capable of stretching and contracting on demand upon a chemical stimulus.[15] In this approach, a double-threaded rotaxane (i.e., [c2]daisy chain, Figure 1a) was used in which the two interlocked strings can glide along one another. By introducing two kinds of specific ligands onto the rotaxane axle, as well as a complementary ligand on the macrocyclic part, either contracted or extended forms can be simply obtained by exchanging the nature of the coordinated metal ions (Cu^{+} or Zn^{2+} in the present case). More recently, two important works published concomitantly by the research groups of Stoddart[16,17] and Grubbs[18] attempted to couple together pH-responsive [c2]daisy chain rotaxanes through "click" polymerization, with the aim of summing the contractions and extensions of the single machines along the polymer chains. However, and in both cases, the low degree of polymerization (DP; average values of 11 and 22, respectively) as well as the low solubility of the resulting oligomers precluded the actuation and characterization of coupled translational motions on mesoscopic scales. Thus, the linear amplification of muscle-like translational molecular motions by orders of magnitude has not been demonstrated experimentally to date, although it has been specifically targeted for a long time.[19]

Herein we describe the design of a pH-triggered muscle-like system in which tailored bistable [c2]daisy chain rotaxanes are combined linearly by taking advantage of a metallosupramolecular polymerization process (Figure 1b). Our approach leads to polymer chains that are sufficiently long and soluble so that micrometric changes of their contour length can be measured upon synchronization of thousands of contractions and extensions. To this end, the target monomer **1** was synthesized by a 13-step pathway starting from commercially available 4-bromobenzyl alcohol (Scheme 1). After acetylation of the alcohol, palladium-catalyzed introduction of the TMS-protected acetylene and subsequent desilylation, compound **4** was reacted with terpyridine triflate **5** in a copper-free Sonogashira coupling to produce acetate **6**. The efficient three-step sequence to introduce the azide group afforded compound **7**, which can then be readily engaged in a copper(I)-catalyzed Huisgen cycloaddition with the previously reported bisalkyne pseudorotaxane **8**.[20a] The final steps of this sequence consist of protecting the terpyridine

[*] G. Du, Dr. E. Moulin, Prof. Dr. N. Giuseppone
SAMS Research Group, University of Strasbourg
Institut Charles Sadron, CNRS
23 rue du Loess, BP 84047, 67034 Strasbourg Cedex 2 (France)
E-mail: giuseppone@unistra.fr
Homepage: http://www-ics.u-strasbg.fr/sams.
Dr. N. Jouault,[+] Prof. Dr. E. Buhler
Matière et Systèmes Complexes (MSC) Laboratory
University of Paris Diderot—Paris VII
UMR 7057, Bâtiment Condorcet, 75205 Paris Cedex 13 (France)
E-mail: eric.buhler@paris7.jussieu.fr
[+] Current address: Department of Chemical Engineering
Columbia University, New York, (USA)

[**] The research leading to these results was funded by the European Research Council under the European Community's Seventh Framework Program (FP7/2007-2013)/ERC Starting Grant agreement no. 257099 (N.G.). We wish to thank the CNRS, the icFRC, and the University of Strasbourg for financial support, and the Laboratoire Léon Brilloin (LLB, CEA, Saclay, France) for beamtime allocation. This work was also supported by a postdoctoral fellowship from the Agence Nationale de la Recherche (ANR-09-BLAN-034-02) (N.J.), and a doctoral fellowship from the Chinese Scholarship Council (G.D.).

Supporting information for this article is available on the WWW under http://dx.doi.org/10.1002/anie.201206571.

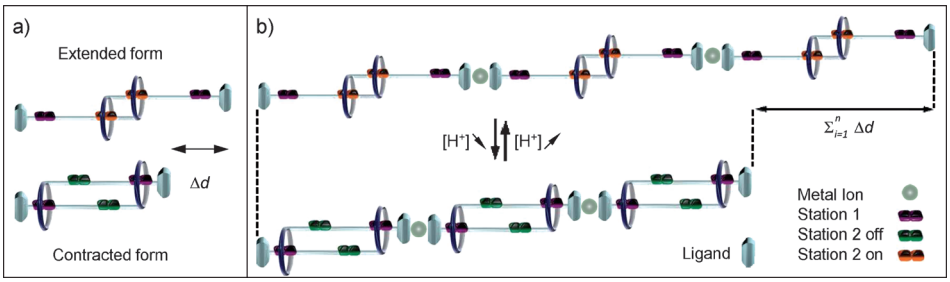

Figure 1. General principle of a) a bistable [c2]daisy chain rotaxane and b) the supramolecular polymer in this study. Here, the stoppers are ligands that can also bind to metal ions to produce coordination polymers. The integrated translational motion of the supramolecular polymer chain is the product of the individual contractions and extensions of each molecular machine by the degree of polymerization.

with copper triflate prior to selective methylation of triazole **9** with iodomethane. The removal of coordinated copper with EDTA followed by the exchange between iodide and hexafluorophosphate counterions gives the desired [c2]daisy chain **1** in an excellent overall yield of 21 %. The bistable nature of this rotaxane is provided by the two binding sites on its axle, that is, the secondary ammonium and the triazolium ions, which are known to have different binding constants with the dibenzo-[24]crown-8 ether.[20b–e] In its protonated form, the ammonium binds to the macrocycle (extended, $\mathbf{1}^{ext}$), whereas in its deprotonated one the crown ether moves to the triazolium site (contracted, $\mathbf{1}^{cont}$), as confirmed by ^{1}H NMR titrations in both directions using either trifluoroacetic acid or sodium hydroxide (Figure S1 in the Supporting Information).

We then turned to the supramolecular polymerizations of $\mathbf{1}^{cont}$ and $\mathbf{1}^{ext}$ by using one equivalent of either $Zn(OTf)_2$ or $FeCl_2$ in a $CDCl_3/CD_3CN$ 1:1 solution ([**1**] = 10 mM). As expected, the ^{1}H NMR spectra of the four resulting products (namely $\mathbf{Zn1}^{cont}$, $\mathbf{Zn1}^{ext}$, $\mathbf{Fe1}^{cont}$, and $\mathbf{Fe1}^{ext}$) were too broad to be informative, although strong shifts could be identified in the terpyridine region, thus indicating a probable binding of the metal ions. This coordination was however unambiguously confirmed by UV/Vis spectra (Figure S2 in the Supporting Information) in which the band that appears around 340 nm in the four solutions, as well as the new charge transfer band at 580 nm for $\mathbf{Fe1}^{cont}$ and $\mathbf{Fe1}^{ext}$ are in agreement with the formation of the bisterpyridine complexes.[21,22]

To further probe the length of the expected supramolecular polymers, as well as their conformation, we have combined a series of light scattering and small-angle neutron scattering (SANS) experiments and extracted key structural parameters (Table 1). SANS is the most powerful method to determine the characteristic sizes and shapes of objects in solution in the range of 1–300 nm. The scattering pattern for a 10 mM solution of $\mathbf{Zn1}^{cont}$, which is below the overlap concentration, is shown in Figure 2a. The product $M_wP(q)$ as a function of the scattered wave vector q[23] was obtained by coupling low-q static light scattering (SLS) and SANS measurements, where M_w is the weight-average molecular

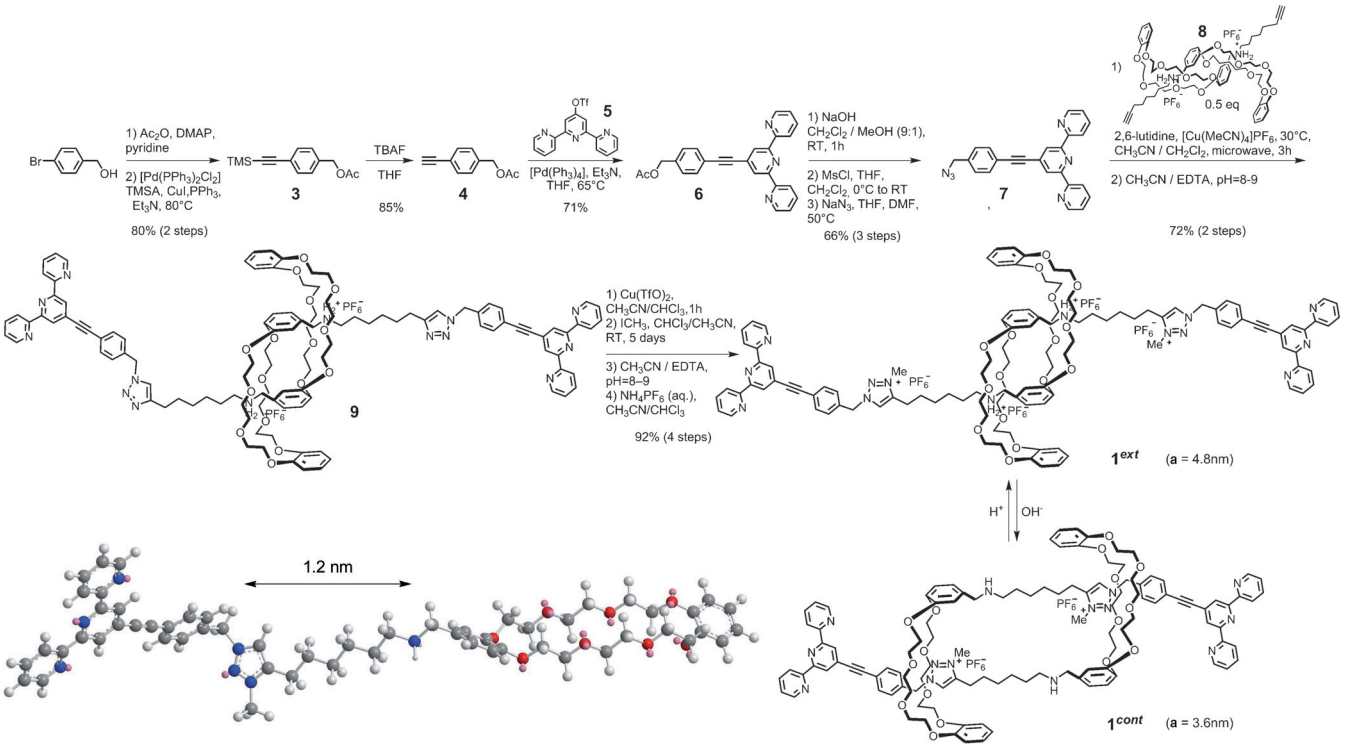

Scheme 1. Synthetic pathway for building monomeric molecular machine **1**. The lengths of $\mathbf{1}^{ext}$ (a = 4.8 nm) and $\mathbf{1}^{cont}$ (a = 3.6 nm), as well as the distance between the two stations (Δd = 1.2 nm), have been determined by molecular modeling. DMAP = 4-dimethylaminopyridine, EDTA = ethylenediaminetetraacetic acid, Tf = trifluoromethanesulfonyl, TMSA = trimethylsilylacetylene.

Table 1: Characteristic structural parameters obtained from the DLS, SLS, and SANS experiments for polymers **Zn1**^{cont}, **Fe1**^{cont}, and **Fe1**^{ext}. a) Theoretical values and b) parameters obtained from the fitting procedure.[a]

a)

	$M°$ [g mol^{-1}][b]	a_{theo} [nm]	$M_{L\,theo}$ [g mol^{-1} nm^{-1}]	Φ[c]
Zn1^{cont}	2334	3.6	648	0.0202
Fe1^{cont}	2395	3.6	665	0.0184
Fe1^{ext}	2687	4.8	559	0.0190

b)

	$M_{w\,fit}$ [×10^6 g mol^{-1}]	DP	L_c [nm]	$L_{c\,theo}$ [nm][d]	$M_{L\,exp}$ [g mol^{-1} nm^{-1}]
Zn1^{cont}	5.179	1967	8854	8261	585
Fe1^{cont}	7.030	2937	9398	10573	748
Fe1^{ext}	7.890	2937	15861	14097	498

	L_p [nm]	$R_{g\,Benoît–Doty}$ [nm][e]	a_{exp} [nm]	R_c [nm]	S [nm^2]	R_h [nm]
Zn1^{cont}	15.5	213	4.5	0.30	1.412	206
Fe1^{cont}	12.8	200	3.2	0.45	1.791	167
Fe1^{ext}	17.6	305	5.4	0.40	1.596	189

[a] According to the optimization of the fitting procedures, the calculation of the contrast and the measurement of the monomer density (see the Supporting Information), we estimate an absolute error within 10% on the characteristic structural parameters of Table 1B. [b] $M°$ = monomer mass. [c] Φ = monomer volume fraction. [d] $L_{c\,theo} = DP\,a_{theo}$. [e] $R_{g\,Benoît–Doty}$ = radius of gyration calculated using the Benoît–Doty expression with the values of L_c and L_p.[24]

weight of the scattered species and $P(q)$ the form factor (see the Supporting Information). The overall behavior shown by the scattering curve can be characterized by the following sequence: 1) the onset of a smooth variation analogous to a Guinier regime at very low q values and associated with the finite size and mass of the objects; 2) a low-q regime in which the q-dependence of the data can be described by a power law with the exponent close to −2, such as in Gaussian coils; 3) a q^{-1} domain at intermediate q values that is characteristic of rigid-rod-like behavior for distances smaller than the persistence length L_p; followed by 4) another Guinier regime associated with the cross-section of the polymers. This ensemble of variations is characteristic of wormlike chain behavior.[24] In such case, scattering data is usually represented by a "Holtzer plot"[25] of the product $M_w P(q) \times q$ as a function of q (Figure 2b), which directly demonstrates the crossover from a rigid-rod-like to a coil-like behavior on a length scale of L_p.

The ensemble of variations shown in Figure 2a,b can be considered as a form factor and fitted satisfactorily by a wormlike chain model (see the Supporting Information) to give persistence length $L_p = (15.5 \pm 1.6)$ nm, linear mass density $M_L = M_w/L_c = (585 \pm 110)$ g mol^{-1} nm, and contour length $L_c = (8854 \pm 900)$ nm. From the data at $q = 0$, a DP value of (1967 ± 190) is obtained (with $DP = M_{w\,fit}/M°$), which is in agreement with the theoretical value expected from the thermodynamic stability of the complex at this concentration. The level of the intermediate q^{-1} regime is controlled by the

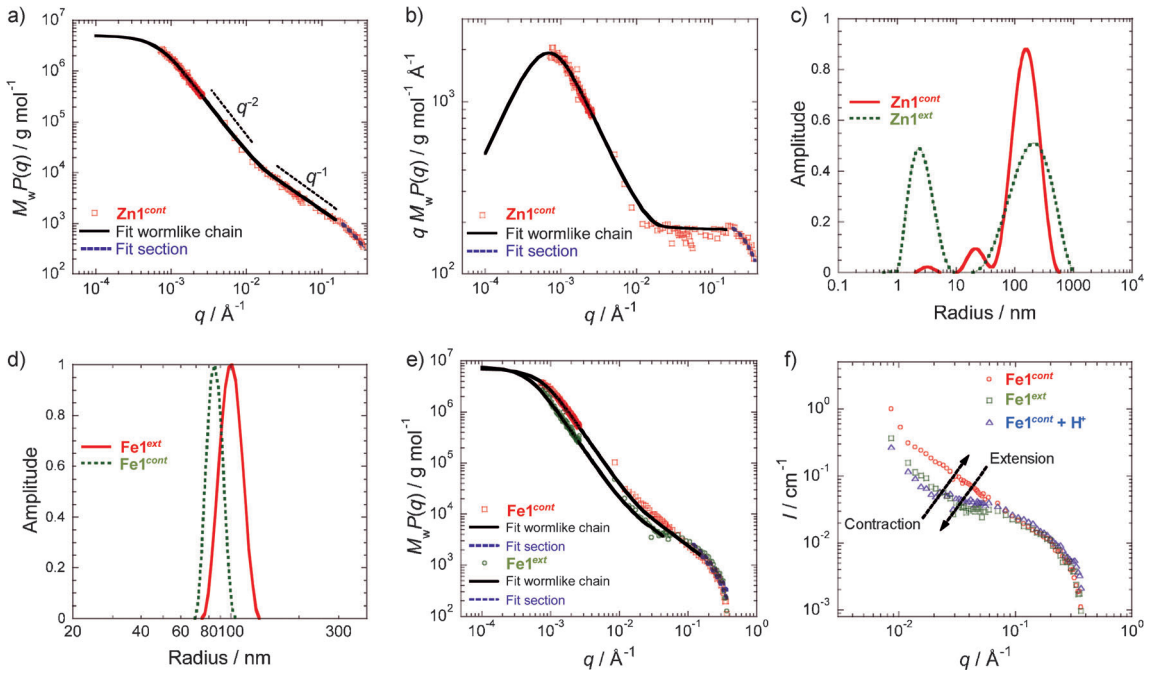

Figure 2. a) Log–log plot of combined SLS and SANS measurements for a solution of **Zn1**^{cont} (10 mM in 1:1 $CDCl_3/CD_3CN$ at $T = 20$°C); b) corresponding Holtzer plot. The continuous line represents the data fit by the wormlike chain model [Eq. (S10) in the Supporting Information] and the dashed line represents the data fit at high q values by a Guinier expression for the form factor of the section [Eq. (S11)]. c) Distribution of the scattering intensity with the R_H values obtained by applying the Contin method to our data at $\theta = 90°$ for Zn-based supramolecular polymers and d) for Fe-based supramolecular polymers. e) SLS and SANS data for **Fe1**^{ext} and **Fe1**^{cont} (10 mM in 1:1 $CDCl_3/CD_3CN$ at $T = 20$°C). The continuous lines represent the best fit of the data by a wormlike chain model [Eq. (S10)] and the dashed line represents the data fit at high q values by a Guinier expression for the form factor of the cross-section [Eq. (S11)]. f) SANS showing only the effect of in situ protonation (2 equiv of CF_3CO_2D) starting from **Fe1**^{cont} and leading to **Fe1**^{ext} compared with the reference of **Fe1**^{ext} polymerized from already extended monomer.

M_L value, which is in excellent agreement with that of a single-strand polymer chain (linear mass density of deprotonated monomer $\mathbf{1}^{cont}$ is $m/a = 2632/3.6 = 731\ g\,mol^{-1}\,nm^{-1}$, where m and a represent the mass and the length of a monomer unit, respectively (Figure S3 and Table S1 in the Supporting Information)). The high-q data has been fitted by a Guinier expression for the form factor of the polymer section, determining the cross-section, $S = (1.42 \pm 0.15)\ nm^2$, and the radius of gyration of the cross-section $R_c = (0.3 \pm 0.03)$ nm, which are in agreement with the monomer section.

As shown by the dynamic light scattering (DLS) results given in Figure 2c, samples of $\mathbf{Zn1}^{ext}$ show a partial depolymerization. The size distribution obtained by applying the Contin analysis to our data shows two populations, one around 2–3 nm, which corresponds to monomers, and another one around 200 nm, which corresponds to polymers. The hydrodynamic radius of the $\mathbf{Zn1}^{cont}$ sample obtained from extrapolation of the data at $q = 0$ is $R_H = (206 \pm 20)$ nm. This observation was confirmed by starting with the preformed polymer and by adding increasing amounts of trifluoroacetic acid, which revealed a competition between protonation and coordination with the Zn ions. To avoid such a drawback, we turned to Fe^{II} ions, which are known to bind even more strongly with terpyridine ligands ($\log\beta = 20.9\ M^{-2}$ in water).[26] Gratifyingly, DLS measurements performed on iron-containing systems indicate the presence of a single polymer population for all deprotonated and protonated samples at various temperatures (Figure 2d and Figure S4 in the Supporting Information). After extrapolation of the data at $q = 0$, $R_H = (167 \pm 17)$ nm for $\mathbf{Fe1}^{cont}$ and $R_H = (189 \pm 19)$ nm for $\mathbf{Fe1}^{ext}$ were determined.

The scattering patterns of $\mathbf{Fe1}^{cont}$ and $\mathbf{Fe1}^{ext}$ in 10 mM solutions are shown in Figure 2e (see Figure S5 in the Supporting Information for scattering patterns at various temperatures). Both samples show the same wormlike-chain behavior that is characterized by the sequence described above for $\mathbf{Zn1}^{cont}$. Scattering variations are fitted satisfactorily by the wormlike-chain model, and we obtained values of $L_p = (12.8 \pm 1.3)$ nm, $M_L = (748 \pm 150)\ g\,mol^{-1}\,nm^{-1}$, $L_c = (9398 \pm 1000)$ nm, and $DP = (2937 \pm 290)$ for $\mathbf{Fe1}^{cont}$ and $L_p = (17.6 \pm 1.8)$ nm, $M_L = (498 \pm 100)\ g\,mol^{-1}\,nm^{-1}$, $L_c = (15861 \pm 1500)$ nm, and $DP = (2937 \pm 290)$ for $\mathbf{Fe1}^{ext}$. The contraction–extension process is clearly demonstrated by these results, as we observe for the $\mathbf{Fe1}^{ext}$ sample: 1) an increase of the contour length of the chain, and 2) a reduction of the linear density. The values of the experimental linear mass densities are in agreement with that calculated for a single-strand contracted chain ($m/a = 665\ g\,mol^{-1}\,nm^{-1}$) and for a single-strand extended chain ($m/a = 559\ g\,mol^{-1}\,nm^{-1}$). Cross-section dimensions for both iron samples correspond to that of a monomer section, thus confirming that no lateral aggregation occurs: $R_c = (0.42 \pm 0.04)$ nm and $S = (1.7 \pm 0.15)\ nm^2$. We have also used SANS to check the effect of the in situ protonation of $\mathbf{Fe1}^{cont}$, which confirms the extension of the supramolecular polymer because, in the q^{-1} regime, the intensity of $\mathbf{Fe1}^{cont} + H^+$ overlaps with the one measured for the sample $\mathbf{Fe1}^{ext}$ prepared by the supramolecular polymerization from already protonated monomer $\mathbf{1}^{ext}$ (Figure 2f).

This work shows, through a number of experimental evidences, that the coupling of thousands of molecular machines along a single polymer chain provides a pathway to integrate their single motions at the mesoscale. The key features of the present system rests on a very efficient metallosupramolecular polymerization of highly functional and bistable [c2]daisy chains that produce perfect wormlike chains. This crucial experimental aspect allows a clear and precise determination of the occurring one-dimensional contraction process, and avoids parasitic effects that would be necessarily brought by cross-chain interactions. The shift between the two SANS curves for $\mathbf{Fe1}^{ext}$ and $\mathbf{Fe1}^{cont}$ is the signature of the relative change in linear mass density between the two samples, and it can be quantified with excellent precision ($\Delta M_L = (250 \pm 25)\ g\,mol^{-1}\,nm$). This local change of the polymer chain is directly correlated with the global change of the polymer contour length ($\Delta L_c = (6.4 \pm 0.7)$ μm; a value which is, by analogy, in the range of the contraction observed in sarcomeres). The measured effect is in good agreement with the expected theoretical value based on the distance between the two stations and on the degree of polymerization. The values also match the experimental SANS values measured on both monomers as references. Thus, this amplification by four orders of magnitude of the mechanical output of thousands of molecular machines linked within a single-strand macromolecular chain, going from nanometers to tens of micrometers, is accessible by combining molecular synthesis, supramolecular engineering, and polymerization processes. The next challenge to access macroscopic responses will consist in varying the persistence length of these single-chain polymers, and in bundling and orienting them in stiffer fibers, just as myofibrils do in muscles.

Received: August 15, 2012
Published online: October 18, 2012

Keywords: molecular machines · nanotechnology · responsive materials · rotaxanes · supramolecular polymers

[1] J.-M. Lehn, *Science* **2002**, *295*, 2400 – 2403.
[2] G. M. Whitesides, B. Grzybowski, *Science* **2002**, *295*, 2418 – 2421.
[3] S. Mann, *Angew. Chem.* **2008**, *120*, 5386 – 5401; *Angew. Chem. Int. Ed.* **2008**, *47*, 5306 – 5320.
[4] J. L. Krans, *Nature Education* **2010**, *3*, 66.
[5] K. Kinbara, T. Aida, *Chem. Rev.* **2005**, *105*, 1377 – 1400.
[6] E. R. Kay, D. A. Leigh, F. Zerbetto, *Angew. Chem.* **2007**, *119*, 72 – 196; *Angew. Chem. Int. Ed.* **2007**, *46*, 72 – 191.
[7] L. Fang, M. A. Olson, D. Benítez, E. Tkatchouk, W. A. Goddard III, J. F. Stoddart, *Chem. Soc. Rev.* **2010**, *39*, 17 – 29.
[8] R. A. Bissell, E. Córdova, A. E. Kaifer, J. F. Stoddart, *Nature* **1994**, *369*, 133 – 137.
[9] B. K. Juluri, A. S. Kumar, Y. Liu, T. Ye, Y.-W. Yang, A. H. Flood, L. Fang, J. F. Stoddart, P. S. Weiss, T. J. Huang, *ACS Nano* **2009**, *3*, 291 – 300.
[10] M. von Delius, E. M. Geertsema, D. A. Leigh, *Nat. Chem.* **2010**, *2*, 96 – 101.
[11] T. Muraoka, K. Kinbara, Y. Kobayashi, T. Aida, *J. Am. Chem. Soc.* **2003**, *125*, 5612 – 5613.
[12] D. A. Leigh, J. K. Y. Wong, F. Dehez, F. Zerbetto, *Nature* **2003**, *424*, 174 – 179.

[13] N. Koumura, R. W. J. Zijistra, R. A. Van Delden, N. Harada, B. L. Feringa, *Nature* **1999**, *401*, 152 – 155.
[14] T. R. Kelly, H. De Silva, R. A. Silva, *Nature* **1999**, *401*, 150 – 152.
[15] M. C. Jiménez, C. Dietrich-Buchecker, J.-P. Sauvage, *Angew. Chem.* **2000**, *112*, 3422 – 3425; *Angew. Chem. Int. Ed.* **2000**, *39*, 3284 – 3287.
[16] L. Fang, M. Hmadeh, J. Wu, M. A. Olson, J. M. Spruell, A. Trabolsi, Y.-W. Yang, M. Elhabiri, A.-M. Albrecht-Gary, J. F. Stoddart, *J. Am. Chem. Soc.* **2009**, *131*, 7126 – 7134.
[17] L. Fang, M. Hmadeh, A. Trabolsi, M. Elhabiri, A.-M. Albrecht-Gary, J. F. Stoddart, *J. Mater. Chem.* **2010**, *20*, 3422 – 3430.
[18] P. G. Clark, M. W. Day, R. H. Grubbs, *J. Am. Chem. Soc.* **2009**, *131*, 13631 – 13633.
[19] B. L. Feringa, *Nature* **2000**, *408*, 151 – 154.
[20] a) F. Coutrot, C. Romuald, E. Busseron, *Org. Lett.* **2008**, *10*, 3741 – 3744; b) F. Coutrot, E. Busseron, *Chem. Eur. J.* **2008**, *14*, 4784 – 4787; c) C. Romuald, A. Ardá, C. Clavel, J. Jiménez-Barbero, F. Coutrot, *Chem. Sci.* **2012**, *3*, 1851 – 1857; d) C. Romuald, E. Busseron, F. Coutrot, *J. Org. Chem.* **2010**, *75*, 6516 – 6531; e) Y. Jiang, J.-B. Guo, C.-F. Chen, *Org. Lett.* **2010**, *12*, 4248 – 4251.
[21] S.-C. Yu, C.-C. Kwok, W.-K. Chan, C.-M. Che, *Adv. Mater.* **2003**, *15*, 1643 – 1647.
[22] H. Hofmeier, R. Hoogenboom, M. E. L. Wouters, U. S. Schubert, *J. Am. Chem. Soc.* **2005**, *127*, 2913 – 2921.
[23] J. Appell, G. Porte, E. Buhler, *J. Phys. Chem. B* **2005**, *109*, 13186 – 13194.
[24] E. Buhler, F. Boué, *Eur. Phys. J. E* **2003**, *10*, 89 – 92.
[25] M. Rawiso, *J. Phys. IV* **1999**, *9* (Pr1), 147 – 195.
[26] A. E. Martell, R. M. Smith, *Critical Stability Constants*, Plenum, New York, **1974**.

